Molecular Physics 111 (2013), 2683-2689
http://dx.doi.org/10.1080/00268976.2013.820361 (†)

RESEARCH ARTICLE

Electrical detection of Rabi oscillations in microcrystalline silicon thin-film solar cells

C. Meier[a], J. Behrends[a*] and R. Bittl[a]

[a] *Fachbereich Physik, Freie Universität Berlin, Arnimallee 14, D-14195 Berlin, Germany*

(*Received 00 Month 200x; final version received 00 Month 200x*)

The microscopic structure of the light-activated paramagnetic CE centre and its participation in spin-dependent hopping transport is studied in a microcrystalline silicon thin-film solar cell. Application of X- and S-band electrically detected magnetic resonance (EDMR) experiments in combination with numerical simulations of Rabi oscillations indicate that the spin-dependent process takes place between two neighbouring CE centres. For sufficiently high microwave power two Rabi frequencies Ω_1 and $\Omega_2 = 2\Omega_1$ show up in the coherent EDMR signals. An analysis of their relative contributions to the Rabi traces suggests that the g-values of both CE spin partners are not correlated for the majority of the EDMR-active pairs. A small fraction of doublet pairs with similar g-values may explain the appearance of a larger Ω_2 contribution than predicted by the simulations.

Keywords: EDMR; Rabi oscillations; microcrystalline silicon; solar cells

1. Introduction

Electrically detected magnetic resonance (EDMR) has evolved as a valuable tool to identify transport and recombination pathways in a wide range of materials and devices. This technique measures changes in the electrical conductivity of a semiconductor arising from manipulation of spin-dependent transition rates that involve paramagnetic states. It thus combines the microscopic selectivity of electron paramagnetic resonance (EPR) with the sensitivity of a current measurement. While early EDMR studies focused on spin-dependent scattering of (delocalised) conduction electrons in crystalline silicon at paramagnetic donors [1–3], subsequent works investigated recombination via localised states such as defect states at silicon surfaces [4]. Since then, the field of application was extended to a large variety of inorganic and organic semiconductors. EDMR has proven successful in elucidating spin-dependent transport and recombination pathways in hydrogenated amorphous silicon (a-Si:H) and hydrogenated microcrystalline silicon (μc-Si:H) and, in particular, thin-film solar cells based on these materials (for a review see Ref. [5] and references therein).

In a continuous wave (cw) EDMR experiment the sample is continuously subjected to microwave (mw) radiation while the current change is detected as function of the magnetic field, resulting in the EDMR spectrum. The g-values and line shapes identify the paramagnetic centres participating in current-determining processes in EDMR, as in conventional EPR, nevertheless often different processes may lead to

*Corresponding author. Email: j.behrends@fu-berlin.de, telephone: 0049 30 83852769, fax number: 0049 30 83856046

indistinguishable EDMR spectra. In this case pulsed (p) EDMR employing short mw pulses [6] can help to pinpoint the microscopic process in two different ways. First, the time behaviour of EDMR signals can reveal which paramagnetic centres are connected via a transport process [7]. Second, coherent effects can be harnessed in a similar way like in pulsed EPR [8, 9]. These coherence effects were recently utilised to identify spin-dependent transport and recombination mechanisms in organic semiconductors based on the frequency components observed in electrically detected Rabi oscillations [10–12].

We apply a similar strategy to investigate spin-dependent charge carrier hopping via conduction band tail states, referred to as *CE centres*, in μc-Si:H. An EDMR signal attributed to CE states is frequently found in the low-temperature transport properties of μc-Si:H films [5, 13] and μc-Si:H-based solar cells [14]. The CE centre is of particular technological relevance because it can influence the photocurrent through trapping and thus affects the charge carrier collection efficiency in thin-film solar cells. Since each spin-dependent transition involves two CE centres, the transport-limiting hopping transition is governed by the properties of a doublet pair [15]. Provided sufficient mw power is available and the g-values of both CE centres are similar, the collective manipulation of both spin partners should result in *spin-locking* behaviour, i.e., in Rabi oscillations with the frequency $\Omega_2 = 2\gamma B_1$ with γ being the gyromagnetic ratio and B_1 the amplitude of the magnetic field induced by the mw radiation [16]. However, previous X-band EDMR experiments showed that the coherent oscillations observed for CE hopping transport are rather dominated by the Rabi frequency $\Omega_1 = \gamma B_1$ as expected for a single $S = 1/2$ centre [14]. A similar behaviour was found for hopping transport through a-Si:H conduction band tail states [17] and for spin-dependent recombination in a-Si:H films [18]. This raises the question whether a significant Ω_2 component can be detected at all in EDMR experiments on thin-film silicon devices. It further gives rise to the question if disorder [19] or strong broadening of the EDMR signature of one spin partner may lead to an effective suppression of the Ω_2 Rabi frequency. Here we report the application of coherent pEDMR spectroscopy using X- and S-band resonance frequencies to study the mw-power dependence of the Rabi oscillations in combination with simulations of the dynamics of weakly-coupled CE spin pairs in order to address these questions.

2. Experiments

2.1. *Materials and Methods*

2.1.1. Sample

The investigated solar cell was produced using 94.7 MHz plasma enhanced chemical vapour deposition (PECVD). The cell was deposited at 260 °C on a glass substrate (Corning 1737) consisting of a stack with 800 nm ZnO TCO, boron-doped p-μc-Si:H, 1 μm intrinsic μc-Si:H absorber, phosphorus-doped n-μc-Si:H, ZnO and silver as a back contact. In order to perform EDMR measurements solar cells of 1×1 mm^2 with a special contact configuration were prepared with laser scribing. The preparation sequence and laser scribing procedure was presented in more details elsewhere [14, 20].

2.1.2. Experiment

All measurements were carried out on a BRUKER E580 spectrometer with a split ring resonator (ER4118S-MS5) and a dielectric ring resonator (EN4118X-MD4), respectively, for the S- and X-band experiments. A combined voltage source

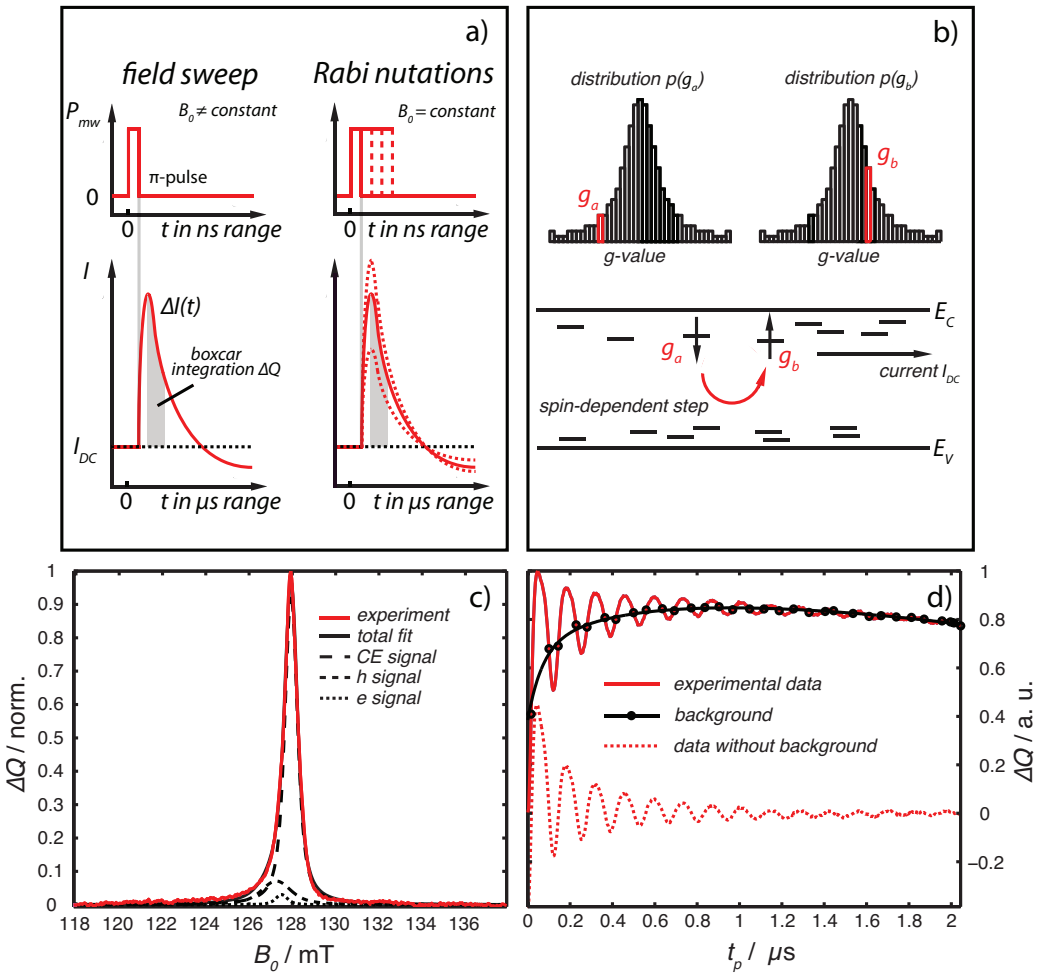

Figure 1. a) Field sweep experiment: At a constant time after the mw π-pulse the current response $\Delta I(t)$ is integrated (yielding ΔQ) and detected as a function of B_0. Rabi experiment: At constant B_0 the pulse length t_p is incremented. At a constant waiting time after the pulse $\Delta I(t)$ is integrated and measured as a function of t_p. b) A scheme of the μc-Si:H band structure with two spins (with g-values g_a and g_b) in localised CE centres near the conduction band (E_C). A spin-dependent process between both spins leads to the EDMR signal. For the simulations both spin-pair constituents are assumed to have g-values g_a and g_b taken from g-distributions $p(g_a)$ and $p(g_b)$. c) Field sweep spectrum measured at S-band showing three EDMR signals. d) Rabi oscillations for $B_1 = 0.26$ mT measured on the maximum of the S-band spectrum.

and current amplifier was used to detect the EDMR signal [14]. With the help of a 1 kW TWT mw amplifier at X-band and a 40 W solid-state amplifier at S-band short π pulses of $t_\mathrm{p} = 20$ ns and 60 ns (excitation bandwidth $\Delta\nu \approx 1/t_\mathrm{p} = 50$ and 17 MHz, which corresponds to 1.4 mT and 0.5 mT, respectively) were generated. The sample cooling was realised by Helium flow cryostats and temperature controllers ITC503 from Oxford Instruments and 321 Autotuning from LakeShore to perform EDMR experiments at 5 K. The solar cell was operated in reverse direction ($U = -1$ V) under illumination with a halogen cold light source (150 W). Illumination through the optical window in the resonator at X-band resulted in a photocurrent of 7.2 μA. At S-band the sample was irradiated via an optical fibre and a small micro-prism delivering 5.5 μA. For all Rabi experiments the current response $\Delta I(t)$ after the mw pulse excitation was boxcar integrated from 3 to 7 μs at S- and from 5 to 9 μs at X-band yielding ΔQ with a high signal-to-noise-ratio.

2.1.3. Simulation of coherent spin motion

The coherent evolution of the doublet pairs with two $S = 1/2$ during a mw pulse was modelled by integrating the Liouville-von Neumann equation

$$\frac{d\rho}{dt} = -i\,[H(t), \rho(t)] \tag{1}$$

using the spin-pair Hamiltonian

$$\begin{aligned} H(t) &= H_0 + H_1(t) \\ &= \frac{\mu_B B_0}{\hbar}\left(g_a S_a^z + g_b S_b^z\right) + \frac{\mu_B B_1}{\hbar}\cos(\omega t)\left(g_a S_a^x + g_b S_b^x\right) \end{aligned} \tag{2}$$

including only the electron Zeeman interaction of both spins as well as the interaction with the mw-induced magnetic field. The spin-pair Hamiltonian consists of a static part, H_0, and a time-dependent part, H_1 (caused by the mw magnetic field). Further, ρ represents the density matrix describing the spin-pair ensemble, $g_{a,b}$ denote the g-values of the spin-pair constituents a and b with spin operators $S_{a,b}$, B_0 is the amplitude of the static magnetic field, and B_1 is the amplitude of the mw field with frequency $\omega/2\pi$ (μ_B: Bohr magneton, $\hbar$: Planck's constant). We assume weakly coupled spin pairs and thus do not take mutual spin-spin interactions (exchange and dipolar coupling) into account. Loss of spin pairs (due to recombination or dissociation) is neglected during the mw pulse and included later by an exponential damping of the simulated EDMR signal.

To account for the finite line width of the CE EDMR signal, which results in a distribution of resonance frequencies, we replaced the g-values in eq. (2) by g-distributions determined from fits to the S-band pEDMR spectrum. Note that the application of this procedure is not restricted to inhomogeneously broadened resonances due to a true distribution of g-values as a consequence of g-strain. It is also valid for line broadening due to unresolved hyperfine interactions. In both cases inhomogeneous broadening leads to a distribution of resonance frequencies that can be covered by the numerical treatment based on a distribution of g-values.

The S-band EDMR spectrum of the CE centre can be approximated by a Lorentzian line profile with a line width (FWHM) of $\Delta B_{1/2} = \Delta B_{\mathrm{CE}}^{\mathrm{S}} = 0.7$ mT. Surprisingly, the line shape is much better approximated by a Lorentzian line than a Gaussian. However, this Lorentzian line shape is not related to a homogeneous lifetime broadening. We thus included the following distribution of g-values

$$p(g_a) = \frac{2}{\pi}\frac{1}{\Delta g_a}\left[1 + 4\left(\frac{g_a - \bar{g}_a}{\Delta g_a}\right)^2\right]^{-1} \quad \text{with } \bar{g}_a = 1.99729 \text{ and } \Delta g_a = 0.0111 \tag{3}$$

with Δg_a being the width (FWHM) of the g-distribution centred at $\bar{g}_a$. The g-distribution is illustrated in Fig. 1 b). We assume that the g-distribution for the other constituent of the spin pair, i.e. $p(g_b)$, is identical to $p(g_a)$ except for the central g-value which was set to $\bar{g}_b = 1.99731$. The marginal offset between $\bar{g}_a$ and $\bar{g}_b$ was introduced because pairs of spins with identical g-values may cause numerical instabilities.

To model the spin-pair dynamics we form spin pairs by taking one spin from $p(g_a)$ and one spin from $p(g_b)$ and calculated the spin pair evolution as a function of the mw pulse length t_{p} by numerically integrating eq. (1) using easyspin's propint function [21]. For 9×10^4 spin pairs with varying g-values (taken from the distributions $p(g_a)$ and $p(g_b)$ consisting of 300 points each) we determine the population of

the product states $|\uparrow\downarrow\rangle$ and $|\downarrow\uparrow\rangle$ with antiparallel spin alignment at the end of the resonant mw pulse under the assumption that all spin pairs are initially ($t_\mathrm{p} = 0$) in a configuration with parallel spins (pure triplet states). We consider the g-values of both paramagnetic centres forming a spin pair to be uncorrelated, meaning any spin from $p(g_a)$ can form a pair with any other spin from $p(g_b)$. The results for all 9×10^4 spin pairs are added up, yielding the ensemble average. The initial condition is based on the premise that pairs with parallel spins live longer than those in pure triplet states [22].
We assume that the pEDMR signal (i.e. the resonant change in conductivity) is proportional to the combined population of the states $|\uparrow\downarrow\rangle$ and $|\downarrow\uparrow\rangle$ after the mw pulse. This corresponds to the sum of the populations of the states $|S\rangle$ and $|T^0\rangle$ in the case of strong intersystem crossing between these states and is thus independent of the chosen basis. Damping of the Rabi oscillations due to gradual loss of spin pairs during the excitation is accounted for by including exponential damping of the oscillation amplitude from the experimental data. Damping due to de-phasing of spin pairs is automatically incorporated in the simulation by including g-value distributions. Depending on the ratio between the width of the g-distributions and the mw power, the Rabi oscillations obtained by averaging over the contributions from all spin pairs are dominated either by the frequency Ω_1 (selective excitation at low mw power) or Ω_2 (spin locking at high mw power).

2.2. *Measurements and Evaluation*

The field sweep EDMR spectra were measured using low power π-pulses of $t_\mathrm{p} = 300$ ns length in a field range of 20 mT at S- and 40 mT at X-band. The S-band spectrum in Fig. 1 c) shows one slightly asymmetric peak near $B_0 = 128$ mT. Application of decomposition techniques making use of the transient dynamics [7, 23] reveals three overlapping resonances. The dominant contribution at $g_\mathrm{CE} \approx 1.998$ (83 % of the integrated spectral intensity and Voigtian line width (FWHM) $\Delta B^\mathrm{S}_\mathrm{CE} = 0.70(3)$ mT) is assigned to conduction band tail states (CE centres) participating in spin-dependent hopping transport in the crystalline regions of the material [7, 14]. Furthermore two minor contributions are found: a Voigtian line at $g_\mathrm{e} \approx 2.004$ with $\Delta B^\mathrm{S}_\mathrm{e} = 0.65(5)$ mT (relative contribution: 2.5 %) which is attributed to conduction band tail states (e states) in the amorphous regions as well as a broad Voigtian line at $g_\mathrm{h} \approx 2.010$ with $\Delta B^\mathrm{S}_\mathrm{h} = 1.63(5)$ mT (relative contribution: 14.5 %) due to valence band tail states (h states) [14]. From S- to X-band the line widths of the contributing signals grow by a factor of ≈ 3 and the line intensities change slightly due to different illumination conditions. Nevertheless we can assume that the EDMR signal is predominantly governed by the CE signal when the magnetic field is set to $B_0 = h\nu / g_\mathrm{CE}\mu_B$ in the Rabi oscillation measurements.
Rabi oscillations were measured in the centre of these field sweep EDMR spectra. The applied mw pulse is incremented in time steps of 2 ns up to a length of 2 and 0.5 µs at S- and X-band, respectively, and the integral of the current response is detected (Fig. 1 a), right side). An example of Rabi oscillations is shown in Fig. 1 d) measured at S-band. For the analysis of the obtained data advanced fitting routines were used, implemented in MATLAB (The Mathworks, Natick, MA, USA). First the non-modulating background of the Rabi data is removed. Afterwards the time traces were apodised by a Hamming window to obtain a high side-band suppression before fast-Fourier transformation (FFT). The resulting frequency spectra are given in Fig. 2 b) and 3 b).

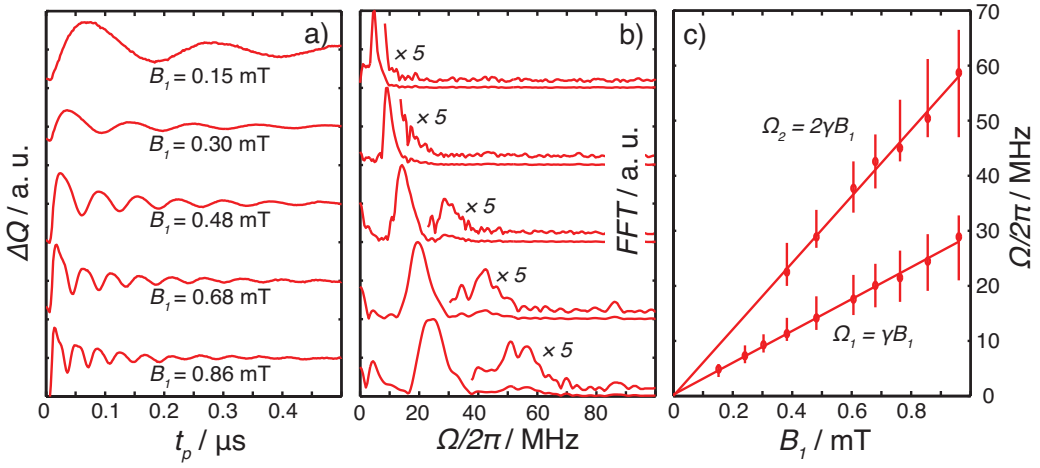

Figure 2. a) and b): Background-free X-band Rabi oscillations for different B_1 field strengths and corresponding FT spectra. c) Oscillation frequencies Ω_1 and Ω_2 deduced from the FT spectra in dependence on B_1. The vertical lines at each frequency point indicate the line widths in the FT spectrum (FWHM).

3. Results and Discussion

3.1. *X-band Rabi oscillations*

In Fig. 2 a) Rabi oscillations at X-band are shown for different mw B_1 fields. In dependence on B_1 the oscillation frequency Ω_1 increases. At high B_1 values the shape of the oscillating signal changes notably. In the FT spectra (Fig. 2 b)) this results in a second component Ω_2, which is hardly visible as a broad line. Strong mw background signals at high B_1 fields reduce the quality of the measurement and lead to broadened lines in the frequency domain. Evaluation of both frequency contributions of all measured Rabi oscillations with B_1 values up to 0.96 mT delivers a linear B_1-dependence for Ω_1 and Ω_2 differing by a factor of 2, which means that $\Omega_2 = 2\Omega_1$ (Fig. 2 c)).
The frequency Ω_1 apparent in all time traces is due to the coherent spin motion of a single CE centre in resonance. The frequency component at Ω_2 measured at high mw field strengths is predicted in the case of small Larmor separation of the two coupled spin partners [22, 24]. This means, we detect a contribution of coupled spin pairs to the EDMR signal. However, the intensity is too weak to allow a more detailed analysis.

3.2. *S-band Rabi oscillations and simulations*

The detection of the second oscillation frequency Ω_2 in Rabi experiments of spin pairs with partners of similar g-values can be further improved by reduction of their Larmor separation. This is achieved at lower mw frequencies. As the CE line width decreases by a factor of 2.6 going from X- to S-band frequencies we have performed Rabi experiments at this lower frequency band. B_1 fields of only up to 0.29 mT are reached in our setup (reduction by a factor of 3.3 in comparison to X-band), nevertheless the quality of the experimental data is enhanced, because the smaller B_1 fields lead to a reduction of the disturbing high power background signals.
The S-band Rabi oscillations for different B_1 fields are shown in Fig. 3 a). The data (red lines) show a high signal-to-noise-ratio revealing the Ω_2 component as a narrow peak in the FT spectra (Fig. 3 b)). The frequencies found show a linear behaviour with slopes differing by a factor of 2 as already found at X-band. For

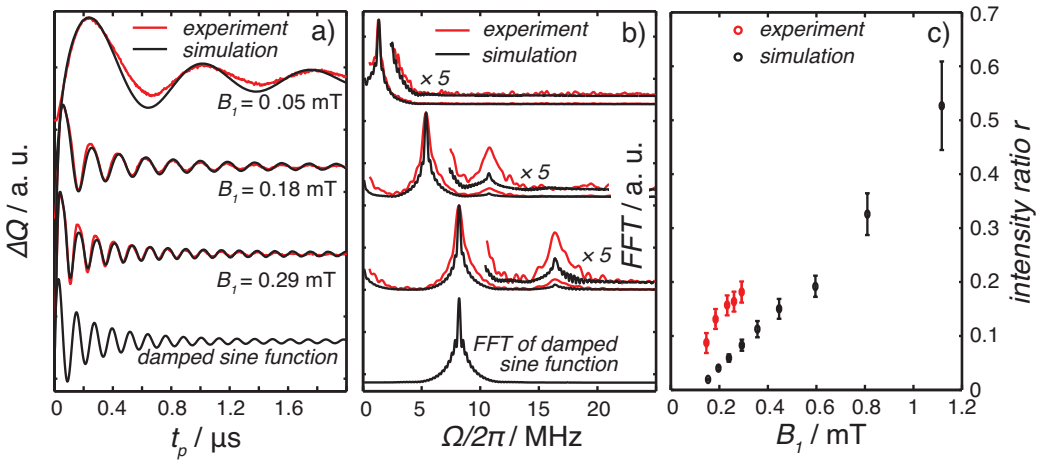

Figure 3. a) Three examples of background-free S-band Rabi oscillations (red) and corresponding simulations (black) for three B_1 fields strengths. A damped sine function is added and evaluated with the same methods to exclude that the Ω_2 signal is due to a numerical artefact. b) FT spectra of experiments, simulated data and sine function. c) Ratio r comparing the intensities S_{Ω_2} and S_{Ω_1} of the two frequency contributions deduced from the experimental and simulated FT spectra as a function of B_1.

three mw field strengths ($B_1 = 0.05$, 0.18 and 0.29 mT) Rabi oscillations were calculated by numerical simulation (shown in black) and post-processed (see Sec. 2.2) to allow a direct comparison with the experimental data. In addition a damped sine function was simulated and evaluated in the same way to show the influence of possible artefacts from the post-processing. For the damped sine function, only a broadened line at the basic frequency arises, showing that the second harmonic is not generated by the post-processing. The simulated Rabi oscillations and their FT spectra are in very good agreement with the experiment. Taking a closer look, the contribution of the Ω_2 component appears weaker in the simulations in comparison to the experimental spectra. To evaluate this aspect, further simulations were performed for B_1 fields up to 1.1 mT. Afterwards both frequency components at Ω_1 and Ω_2 were approximated with symmetric lines for a good fit of all FT spectra and to obtain their line intensities S_{Ω_1} and S_{Ω_2}. The line intensity ratio $r = S_{\Omega_2}/S_{\Omega_1}$ was compared as a function of B_1. The results are displayed in Fig. 3 c). With decreasing B_1 fields the relative Ω_2 contribution becomes smaller in experiment and simulation, as the reduced excitation bandwidth reduces the probability to excite both spin partners with different g-values in the g-distributions. However, the relative contribution of the higher frequency found in the measured data exceeds the contribution deduced from the simulated data by a factor of roughly 2. This high proportion of the Ω_2 line allows to answer the question regarding the spin partner of the CE centre. As the e and h signals contribute by less than 5% to the EDMR spectrum (Fig. 1 c)) at the field position where the Rabi oscillations were recorded, one would expect a strong reduction of the Ω_2 component. Hence these states can be excluded as partners of the CE centre. Thus we conclude that the EDMR signal at $g_{\mathrm{CE}} \approx 1.998$ is due to spin-dependent transport via neighbouring CE centres. A possible origin of the discrepancy between $r = S_{\Omega_2}/S_{\Omega_1}$ in experiment and simulation will be analysed in the following.

3.3. *Influence of the line width*

Even though the experimental proportion of the Ω_2 component in the time traces is roughly a factor 2 larger than in the simulation, its intensity is too low to show a discernible frequency component directly in the Rabi oscillations traces and shows up clearly only in the FT (Fig. 3 b)). This is in contrast to electrically detected

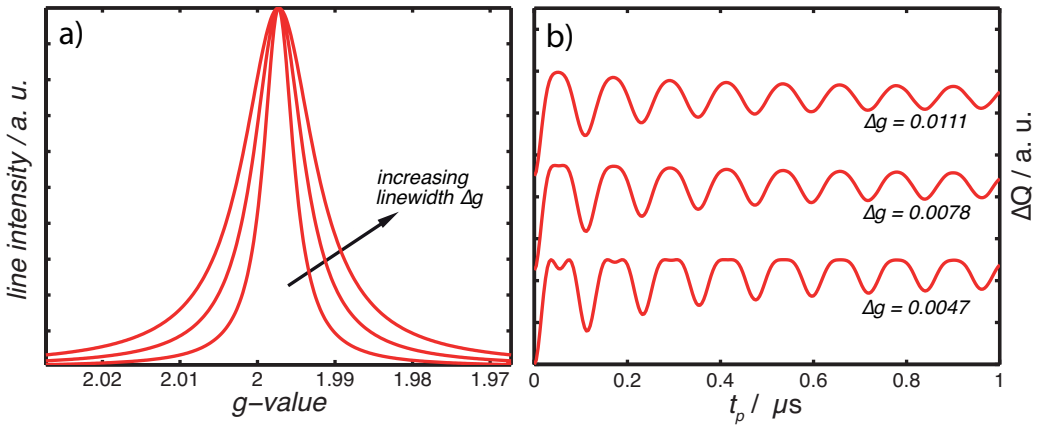

Figure 4. a) Three g-distributions with line widths of $\Delta g = 0.0047$, 0.0078 and 0.0111 (FWHM) are shown. These values correspond to $\Delta B_{1/2} = 0.3$, 0.5 and 0.7 mT, respectively. b) Simulations of Rabi oscillations for these three line widths.

Rabi oscillations measured on devices made from organic semiconductors such as Zinc phthalocyanine [10], polymers [11] or polymer:fullerene blends [12], where the Ω_2 component is already evident from the Rabi oscillation signal in the time domain. This can be attributed to the line width of the paramagnetic centres causing the EDMR signals in these materials, which is considerably smaller than for the CE line width in μc-Si:H. In consequence, the mw power typically available for X-band EDMR is sufficient to obtain a substantial spin-locking signal for organic semiconductor devices.

In order to study the influence of the EDMR line width on the Rabi oscillations we varied the width of the g-distributions used in the simulation. Fig. 4 b) shows the simulation results for $B_1 = 0.29$ mT (the highest B_1 available in our S-band setup) assuming different line widths as illustrated in Fig. 4 a). The uppermost trace corresponds to a CE line width of $\Delta B_{1/2} = \Delta B_{\mathrm{CE}}^{\mathrm{S}} = 0.7$ mT extracted from the S-band EDMR spectrum. Upon decreasing the width of the g-distribution in the simulation, the shape of the maxima of the time domain signal exhibit notable changes until the spin-locking component becomes clearly visible for $p(g_{a,b})$ equivalent to $\Delta B_{1/2} = 0.3$ mT (lowermost curve in Fig. 4). The results show that it is indeed the relatively broad resonance line of the CE centre which impairs the detection of a clear spin-locking feature in the time domain signal for the mw power available in our S-band EDMR setup.

One possibility to increase the intensity of the Ω_2 component is certainly the use of more intense mw pulses without changing the resonance frequency. Another appealing option is to perform EDMR measurements on a high-power EPR spectrometer operating at W-band frequency [25]. Although substantial g-strain will cause the CE line width to be much larger than in S-band, the use of a kilowatt W-band mw amplifier can overcompensate this effect. In addition, the better spectral resolution of the CE signal will provide the possibility to check whether all parts of the g-distribution contribute to the Ω_1 and Ω_2 components in the same way or give rise to different Ω_2/Ω_1 ratios.

4. Conclusions

The comparison between the results of coherent S-band EDMR measurements and numerical simulations indicates that a spin-dependent transition between two paramagnetic centres taken from an inhomogeneously broadened g-value distribution can lead to selective-excitation behaviour in the Rabi oscillation signal, even though

the g-value distribution is assumed to be identical for both centres. The intensity ratio between the Ω_1 and Ω_2 Rabi frequency components as shown in Fig. 3 c) agrees well with the simulation results for uncorrelated spin pairs, corroborating our hypothesis that g_b is independent of g_a for the vast majority of the doublet pairs. However, the experimental values exhibit a systematically stronger spin-locking component than predicted by the simulations for all chosen values of B_1. This may be explained by the following scenario based on the coexistence of two different types of spin pairs.

Most doublet pairs (A) are uncorrelated and lead to the Ω_2/Ω_1 ratio in agreement with the simulation results. Additionally, a second kind of pairs (B) consisting of paramagnetic centres with similar g-values may give rise to a second contribution that is dominated by Rabi oscillations with frequency Ω_2 and thus increases the intensity of this frequency component in the total EDMR signal.

Such a two-component nature of the EDMR signal could be related to the microscopic structure of μc-Si:H [26, 27]. A previous study has shown that the environment of the EDMR-active CE centres is depleted from hydrogen, i.e. the CE centres are located inside crystalline grains [28]. It has recently been suggested that the asymmetric CE EDMR line shape, which is particularly pronounced in Q- and W-band spectra, results from the size distribution of the Si crystallites in μc-Si:H due to a correlation between crystal diameter and CE g-value as a signature of a quantum size effect [23]. Following this idea and further assuming that the diameters of neighbouring Si crystals are not correlated, this model readily explains the fact that the spin-dependent hopping transition between adjacent CE centres localised in two different grains (forming a spin pair of type A) can be attributed to doublet pairs with uncorrelated g-values. On the other hand, Si crystallites with a diameter above a certain threshold may accommodate several CE centres. An intra-grain hopping transition between two such paramagnetic centres (forming a spin pair of type B) produces a spin-locking Rabi oscillation signal. In total, the combined contributions from A and B pairs result in the Ω_2/Ω_1 ratio found in the experiment.

While this model provides a credible explanation for experimental results, other effects can equally affect the behaviour of the Rabi oscillation signals. We note that dipolar and exchange coupling between the spin-pair constituents can severely affect the Ω_2/Ω_1 ratio [29–31]. Since spin-spin couplings are not field-dependent, we believe that coherent EDMR experiments using higher resonance frequencies (Q- and W-band and possibly even higher frequencies) can be applied to distinguish between effects due to g-value distributions and those arising from the presence of spin-spin couplings.

Acknowledgement

We are grateful to O. Astakhov and F. Finger (Forschungszentrum Jülich) for sample preparation as well as to K.-P. Dinse (FU Berlin), Alexander Schnegg and Klaus Lips (Helmholtz-Zentrum Berlin) for helpful discussions. Financial support from BMBF (EPR-Solar network project 03SF0328) is acknowledged.

References

[1] A. Honig, Phys. Rev. Lett. **17** (4), 186 (1966).
[2] R. Maxwell and A. Honig, Phys. Rev. Lett. **17** (4), 188 (1966).
[3] J. Schmidt and I. Solomon, Compt. Rend. Acad. Sci. B **263** (2), 169 (1966).

[4] D.J. Lepine, Phys. Rev. B **6** (2), 436 (1972).
[5] M. Stutzmann, M.S. Brandt and M.W. Bayerl, J. Non-Cryst. Solids **266-269**, 1 (2000).
[6] C. Boehme and K. Lips, Appl. Phys. Lett. **79** (26), 4363 (2001).
[7] J. Behrends, A. Schnegg, C. Boehme, S. Haas, H. Stiebig, F. Finger, B. Rech and K. Lips, J. Non-Cryst. Solids **354** (19-25), 2411 (2008).
[8] C. Boehme and K. Lips, Phys. Rev. Lett. **91** (24), 246603 (2003).
[9] A.R. Stegner, C. Boehme, H. Huebl, M. Stutzmann, K. Lips and M.S. Brandt, Nature Phys. **2** (12), 835 (2006).
[10] S. Schaefer, S. Saremi, K. Fostiropoulos, J. Behrends, K. Lips and W. Harneit, Physica Status Solidi B **245** (10), 2120 (2008).
[11] D.R. McCamey, K.J. van Schooten, W.J. Baker, S.Y. Lee, S.Y. Paik, J.M. Lupton and C. Boehme, Phys. Rev. Lett. **104** (1), 017601 (2010).
[12] J. Behrends, A. Schnegg, K. Lips, E.A. Thomsen, A.K. Pandey, I.D.W. Samuel and D.J. Keeble, Phys. Rev. Lett. **105** (17), 176601 (2010).
[13] W. Fuhs, P. Kanschat and K. Lips, Journal of Vacuum Science & Technology B **18** (3), 1792 (2000).
[14] J. Behrends, A. Schnegg, M. Fehr, A. Lambertz, S. Haas, F. Finger, B. Rech and K. Lips, Philos. Mag. **89** (28-30), 2655 (2009).
[15] D. Kaplan, I. Solomon and N.F. Mott, Journ. de Phys. Lettr. **39** (4), L51 (1978).
[16] Y.N. Molin, O.A. Anisimov, V.M. Grigoryants, V.K. Molchanov and K.M. Salikhov, J. Phys. Chem. **84** (14), 1853 (1980).
[17] C. Boehme, J. Behrends, K. Von Maydell, M. Schmidt and K. Lips, J. Non-Cryst. Solids **352** (9-20), 1113 (2006).
[18] T.W. Herring, S..Y. Lee, D.R. McCamey, P.C. Taylor, K. Lips, J. Hu, F. Zhu, A. Madan and C. Boehme, Phys. Rev. B **79** (19), 195205 (2009).
[19] C. Michel, A. Gliesche, S.D. Baranovskii, K. Lips, F. Gebhard and C. Boehme, Phys. Rev. B **79** (5), 052201 (2009).
[20] S. Haas, A. Gordijn and H. Stiebig, Prog. Photovoltaics **16** (3), 195 (2008).
[21] S. Stoll and A. Schweiger, J. Magn. Reson. **178** (1), 42 (2006).
[22] C. Boehme and K. Lips, Phys. Rev. B **68** (24), 245105 (2003).
[23] C. Meier, J. Behrends, C. Teutloff, O. Astakhov, A. Schnegg, K. Lips and R. Bittl, J. Magn. Res., in press (2013).
[24] Y. Araki, K. Maeda and H. Murai, Chem. Phys. Lett. **332** (5-6), 515 (2000).
[25] P.A.S. Cruickshank, D.R. Bolton, D.A. Robertson, R.I. Hunter, R.J. Wylde and G.M. Smith, Rev. Sci. Instrum. **80** (10), 103102 (2009).
[26] M. Luysberg, P. Hapke, R. Carius and F. Finger, Philos. Mag. A **75** (1), 31 (1997).
[27] L. Houben, M. Luysberg, P. Hapke, R. Carius, F. Finger and H. Wagner, Philos. Mag. A **77** (6), 1447 (1998).
[28] M. Fehr, J. Behrends, S. Haas, B. Rech, K. Lips and A. Schnegg, Phys. Rev. B **84** (19), 193202 (2011).
[29] M. Gierer, A. van der Est and D. Stehlik, Chem. Phys. Lett. **186** (2-3), 238 (1991).
[30] M.E. Limes, J. Wang, W.J. Baker, S..Y. Lee, B. Saam and C. Boehme, Physical Review B **87** (16), 165204 (2013).
[31] R. Glenn, M.E. Limes, B. Saam, C. Boehme and M.E. Raikh, Physical Review B **87** (16), 165205 (2013).